Momentum-resolved linear dichroism in bilayer MoS_2

Klara Volckaert,[1,*] Habib Rostami,[2,*] Deepnarayan Biswas,[3] Igor Marković,[3,4] Federico Andreatta,[1] Charlotte E. Sanders,[5] Paulina Majchrzak,[5] Cephise Cacho,[5] Richard T. Chapman,[5] Adam Wyatt,[5] Emma Springate,[5] Daniel Lizzit,[6] Luca Bignardi,[6,†] Silvano Lizzit,[6] Sanjoy K. Mahatha,[1] Marco Bianchi,[1] Nicola Lanata,[1] Phil D. C. King,[3] Jill A. Miwa,[1] Alexander V. Balatsky,[2] Philip Hofmann,[1] and Søren Ulstrup[1,‡]

[1] *Department of Physics and Astronomy, Interdisciplinary Nanoscience Center, Aarhus University, 8000 Aarhus C, Denmark*
[2] *Nordita, Center for Quantum Materials, KTH Royal Institute of Technology and Stockholm University, Roslagstullsbacken 23, SE-106 91 Stockholm, Sweden*
[3] *SUPA, School of Physics and Astronomy, University of St Andrews, St Andrews KY16 9SS, United Kingdom*
[4] *Max Planck Institute for Chemical Physics of Solids, Nöthnitzer Str. 40, 01187 Dresden, Germany*
[5] *Central Laser Facility, STFC Rutherford Appleton Laboratory, Harwell 0X11 0QX, United Kingdom*
[6] *Elettra-Sincrotrone Trieste, S.S. 14 Km 163.5, Trieste 34149, Italy*

In solid state photoemission experiments it is possible to extract information about the symmetry and orbital character of the electronic wave functions via the photoemission selection rules that shape the measured intensity. This approach can be expanded in a pump-probe experiment where the intensity contains additional information about interband excitations induced by an ultrafast laser pulse with tunable polarization. Here, we find an unexpected strong linear dichroism effect (up to 42.4%) in the conduction band of bilayer MoS_2, when measuring energy- and momentum-resolved snapshots of excited electrons by time- and angle-resolved photoemission spectroscopy. We model the polarization-dependent photoemission intensity in the transiently-populated conduction band using the semiconductor Bloch equations. Our theoretical analysis reveals a strongly anisotropic momentum-dependence of the optical excitations due to intralayer single-particle hopping, which explains the observed linear dichroism.

Optical selection rules in absorption experiments are powerful tools that can be used to determine the symmetry of electronic states in solids [1]. Given the similarity of the processes underlying optical absorption and photoemission, selection rules have also been exploited in angle-resolved photoemission spectroscopy (ARPES) for decades [2]. More recently, optical dichroism has been used in ARPES to study orbital degrees of freedom [3–5], as well as the Berry curvature of the initial Bloch states [6, 7]. A particularly interesting opportunity for polarization-dependent excitations arises in single-layer (SL) transition metal dichalcogenides (TMDCs) such as MoS_2, where the helicity of circularly polarized light strongly couples to the valley and spin degrees of freedom [8, 9], permitting the generation of a finite valley polarization [10, 11].

Adding time-resolution (TR) to ARPES in a pump-probe experiment leads to a process involving two optical excitations. This opens the possibility of exploiting not only the selection rules governing the photoemission process, but also those giving rise to the initial optical excitation into a transiently populated conduction band (CB) state [12–18]. Indeed, the creation of a finite valley-polarization in SL WS_2 has recently been followed in momentum space by TR-ARPES using circularly polarized pump pulses [19, 20]. Here, we extend such an experiment to the case of bilayer (BL) MoS_2 in the 2H structure, which is inversion-symmetric due to the relative orientation of the two layers. Surprisingly, we observe a substantial pump-induced linear dichroism effect for photoemission from the excited states near the conduction band minimum (CBM). Our results can be explained in terms of the momentum-dependent excited state population determined by solving the semiconductor Bloch equations within the framework of a low energy $\boldsymbol{k} \cdot \boldsymbol{p}$ model that accounts for intra- and interlayer interactions between the d orbitals forming the valence band maximum (VBM) and CBM around $\bar{\mathrm{K}}$ ($\bar{\mathrm{K}}'$). These findings underline the necessity of accounting for selection rules governing the optical excitation in addition to the photoemission matrix elements when interpreting the intensity in dichroic TR-ARPES. They also open the possibility to exploit a combination of selection rules to obtain new information about the wave functions involved in the processes.

Our BL MoS_2 sample is grown on Ag(111) and has predominantly one domain orientation, as determined by X-ray photoelectron diffraction measurements [22]. Further details are available in the Supplemental Material [23], which includes Refs. [24–30]. TR-ARPES spectra are collected in the ultra-high vacuum end-station at the Artemis Facility at the Central Laser Facility using the scattering geometry depicted in Fig. 1(a) [23]. A 32.5 eV probe pulse with a linear polarization fixed parallel to the scattering plane is used, following an optical excitation with a 2 eV pulse. The time resolution is 40 fs and the sample temperature is 300 K. We tune the polarization of the pump pulse to obtain arbitrary elliptical polarizations, including linear parallel (p) and perpendicular (s), with respect to the scattering plane. TR-ARPES measurements have been performed near either $\bar{\mathrm{K}}'$ or $\bar{\mathrm{K}}$ by an azimuthal rotation of the sample.

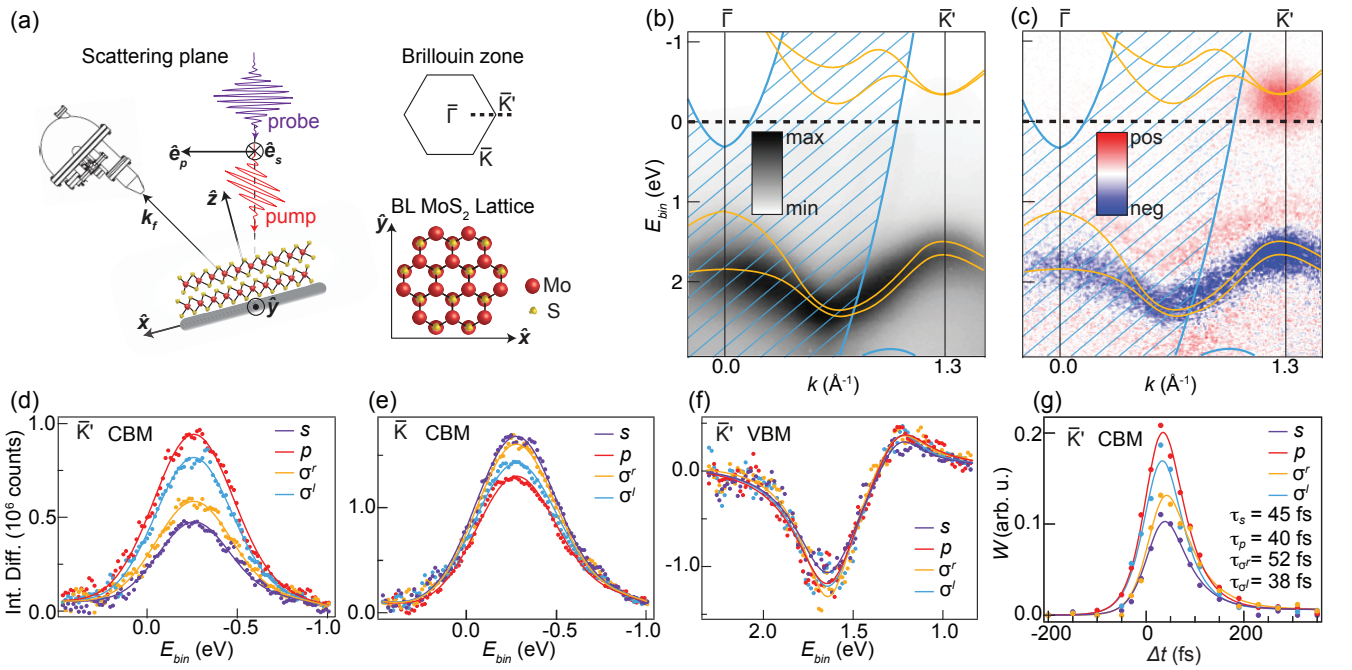

FIG. 1. (a) TR-ARPES setup: Geometry of the scattering plane with definitions of coordinate system $\{\hat{\boldsymbol{x}}, \hat{\boldsymbol{y}}, \hat{\boldsymbol{z}}\}$, photoelectron wavevector $\boldsymbol{k}_f$ and polarization vectors $\{\hat{\boldsymbol{e}}_p, \hat{\boldsymbol{e}}_s\}$ of the light pulses. The orientations of the BL MoS_2 lattice and the Brillouin zone (BZ) are shown for the measurement geometry. The dashed line on the BZ marks the measurement direction. (b) ARPES intensity along the $\bar{\Gamma}$-$\bar{K}'$ high symmetry direction before arrival of the pump pulse ($\Delta t < 0$). (c) Intensity difference between the spectrum in (b) and one obtained at the peak of the optical excitation at $\Delta t = 40$ fs with a s-polarized pump pulse. The dispersion of BL MoS_2 has been overlaid (orange curves) together with the bulk continuum of Ag(111) [21] (blue hatched area) in (b)-(c). (d)-(f) EDCs of the intensity difference for different pump polarizations, fitted with Gaussian peaks for the CBM at (d) $\bar{K}'$ and (e) $\bar{K}$, respectively, as well as (f) for the VBM at $\bar{K}'$. (g) Time dependence of the estimated spectral weight W from (d) fitted with a function composed of an exponential rise and a single exponential decay with the given time constants τ_i.

The photoemission intensity at a time delay, Δt, before excitation ($\Delta t < 0$) is shown in Fig. 1(b). The spectrum mainly resembles the bare dispersion of BL MoS_2 (orange curves) [31] while the intensity from the Ag(111) bulk states (expected in the blue hatched area) is very faint. The intensity of the global VBM of BL MoS_2 (upper band at $\bar{\Gamma}$) is strongly suppressed at the energy of the probe pulse, but it is clearly visible at higher photon energies when measured with static ARPES [23, 32]. Figure 1(c) displays the intensity difference between the equilibrium spectrum in panel (b) and an excited state spectrum collected at the peak of optical excitation at $\Delta t = 40$ fs with a s-polarized pump pulse. The dominant features are a strong excitation of electrons around the local CBM at $\bar{K}'$ (positive intensity difference) and an excitation of holes that peaks at the local VBM at $\bar{K}'$ (negative intensity difference). The red/blue intensity difference associated with the rest of the valence band (VB) is mainly caused by a linewidth broadening of the entire band, which is induced by the pump pulse as observed in TR-ARPES measurements of other materials [33]. From these data we extract an indirect gap of (1.49±0.06) eV from $\bar{\Gamma}$ to $\bar{K}'$ and a direct gap at $\bar{K}'$ of (1.90±0.04) eV, which is close to resonant with our 2 eV optical excitation.

Energy distribution curves (EDCs) of the intensity difference in the CBM averaged over a momentum range from -0.2 to 0.2 $Å^{-1}$ around $\bar{K}'$ are shown with Gaussian fits for s- and p-polarized pump pulses in Fig. 1(d). EDCs are also shown for polarizations generated by rotations of the half-waveplate midway between s- and p-polarizations, which we assume to be circular and therefore label σ^l and σ^r [23]. A strong change is visible between the intensity difference spectra of s- and p-polarized pulses, while a smaller change is seen between σ^l- and σ^r-polarizations. We quantify dichroism as $\rho_{ij} = (W(i) - W(j))/(W(i) + W(j))$, where $i \neq j$ labels s- and p- or σ^l- and σ^r-polarization and W represents the corresponding spectral weight, determined as the area of the EDC fits. At $\bar{K}'$ we then obtain $\rho_{ps} = 42.4$ % and $\rho_{\sigma^l\sigma^r} = 19.7$ %. A similar EDC analysis for the CBM at $\bar{K}$ is presented in Fig. 1(e) and exhibits a reversal and reduction of the linear dichroism effect with $\rho_{ps} = -15.2$ % and likewise $\rho_{\sigma^l\sigma^r} = -4.7$ %. EDCs of the VBM at $\bar{K}'$ in Fig. 1(f) do not permit us to clearly distinguish dichroism from the overall noise level in this spectral region.

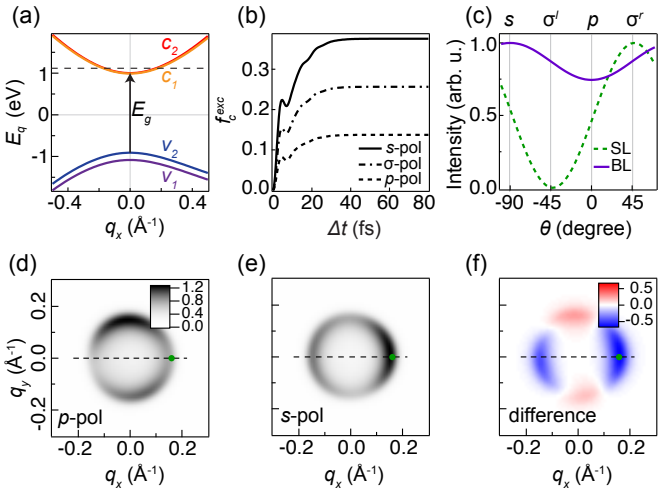

FIG. 2. (a) BL MoS_2 dispersion around $\bar{K}$ determined within a $\boldsymbol{k}\cdot\boldsymbol{p}$ model. The energy split VB states are labeled v_1 and v_2 and the CB states are labeled c_1 and c_2. The direct band gap of $E_g = 1.9$ eV is marked by an arrow. (b) Optically induced population in the CB states obtained at $\boldsymbol{q} = (0.16, 0)$ Å^{-1} (indicated by the green dot in (d)-(f)) by solving the semiconductor Bloch equations for p-, σ- and s-polarized light. (c) Photoemission intensity calculated at $q_y = 0$ and q_x-averaged from -0.22 to 0.22 Å^{-1}, as shown by the dashed black line in (d)-(f), as a function of pump pulse polarization θ for SL MoS_2 (dashed green) and BL MoS_2 (solid purple). (d)-(e) Momentum-dependent photoemission intensity calculated for (d) p- and (e) s-polarized pump pulses. The color scale in (d) also applies to (e). (f) Intensity difference obtained by subtracting the data in (e) from that in (d). The constant energy cuts in (d)-(f) were obtained at $E_q = 1.15$ eV as shown via a dashed horizontal line in (a).

We speculate that ultrafast momentum relaxation of the holes involving the remaining VB states leads to a loss of polarization information of the holes on a faster timescale than we can resolve with our experimental setup.

The time- and polarization-dependence of the spectral weight W at $\bar{K}'$ is shown in Fig. 1(g). In all cases we find that the decay part is well described by single exponentials with the time constants τ_i given in Fig. 1(g). The values of τ_i are similar for all cases and indicate that the carriers are rapidly scattered into the metal substrate [16, 33]. The excitation signal is detectable up to 300 fs while the dichroic signal exceeds the noise level for only 85 fs.

We seek an explanation of the measured dichroism by calculating the polarization-dependent photoemission intensity from the transiently populated CB around $\bar{K}$. A full account of the theory is given in Ref. 34. As a simplified expression we use

$$\mathcal{I}_n(E, \boldsymbol{q}, \theta) \propto |\mathcal{M}_n(\boldsymbol{q})|^2 \mathcal{A}_n(E, \boldsymbol{q}) f_n^{exc}(\boldsymbol{q}, \theta), \qquad (1)$$

where $\mathcal{A}_n$ is the photohole spectral function and f_n^{exc} is the excited state population in the CBs, which we treat as two-fold degenerate and label with the index $n \in \{c_1, c_2\}$ where c_1 and c_2 are the two states. The wave vector is measured from $\bar{K}$ and expressed as $\boldsymbol{q} = (q_x, q_y)$ in units of $\sqrt{3}/a$ where $a = 3.16$ Å is the MoS_2 lattice constant. The one-electron dipole matrix element ($\mathcal{M}_n$) describing photoemission from the CB near $\bar{K}$ is determined by the simple assumption that the initial Bloch state (ψ_n) is matched to a single free-electron final state in the photoemission process. This assumption leads to the expression $\mathcal{M}_n(\boldsymbol{q}) \propto \hat{\boldsymbol{e}}_p \cdot \boldsymbol{k}_f \langle \boldsymbol{k}_f | \psi_n(\boldsymbol{q}) \rangle$, where $\hat{\boldsymbol{e}}_p$ is the polarization unit vector of the probe pulse (see Fig. 1(a)) and $\boldsymbol{k}_f$ is the wavevector of the free electron [34, 35]. The wave functions and dispersion are determined by diagonalizing a $\boldsymbol{k}\cdot\boldsymbol{p}$ Hamiltonian given by

$$\hat{\mathcal{H}}_{\mathrm{BL}}(\boldsymbol{q}, \tau_z, s_z) = \begin{bmatrix} \hat{\mathcal{H}}_{\mathrm{SL}}(-\boldsymbol{q}, -\tau_z, s_z) & \hat{\mathcal{H}}_{\perp}(\boldsymbol{q}, \tau_z) \\ \hat{\mathcal{H}}_{\perp}^{\dagger}(\boldsymbol{q}, \tau_z) & \hat{\mathcal{H}}_{\mathrm{SL}}(\boldsymbol{q}, \tau_z, s_z) \end{bmatrix}, \qquad (2)$$

where $\hat{\mathcal{H}}_{\mathrm{SL}}$ is the Hamiltonian for SL MoS_2 including trigonal warping effects [36–38], and $\hat{\mathcal{H}}_{\perp}$ accounts for the weak interlayer interaction in BL MoS_2 [23, 39, 40]. Furthermore, $\tau_z = \pm 1$ and $s_z = \pm 1$ denote the valley and spin indices, respectively. The corresponding dispersion relation is presented in Fig. 2(a).

To simulate the transient CB population generated by the pump pulse we model the electric field as an ultrashort pulse given by $\boldsymbol{\mathcal{E}}(\Delta t) = \hat{\boldsymbol{\epsilon}}(\theta)\mathcal{E}_0 \cos(\omega_0 \Delta t) e^{-\left(\frac{\Delta t}{\tau_0}\right)^2}$, where $\hat{\boldsymbol{\epsilon}}(\theta) = \hat{\boldsymbol{e}}_p \cos\theta + \mathrm{i}\,\hat{\boldsymbol{e}}_s \sin\theta$ is the polarization of the pump pulse with unit vectors $\hat{\boldsymbol{e}}_p$ and $\hat{\boldsymbol{e}}_s$ defined according to the scattering geometry in Fig. 1(a). Experimental values are used as input for the electric field strength $\mathcal{E}_0 = 0.87$ V/nm (determined by the measured pump spot size and fluence), the pulse energy $\hbar\omega_0 = 2.0$ eV and the pulse duration $\tau_0 = 30$ fs. We then solve the semiconductor Bloch equations [41] as described in detail in Ref. 34, and obtain the excited CB population shown in Fig. 2(b). There is no decrease of the excited state population in time as we have neglected any relaxation processes. As we shall see below, the dichroism in the excited state vanishes exactly at $\bar{K}$. The plot has therefore been made at the point $\boldsymbol{q} = (0.16, 0)$ Å^{-1}, which clearly reveals a strong polarization-dependence of the population at finite $\boldsymbol{q}$. The noticeable cusps in the early stages of the excitation are strongly dependent on the model parameters and are not considered in further detail here since they can not be resolved in our experiment. For the resonance condition $|\hbar\omega_0 - E_g| \ll \hbar/\tau_0$ around $\bar{K}$ (i.e. small q), we can write the population as [34]

$$f_n^{exc}(\boldsymbol{q}, \theta) \approx \left(\frac{\sqrt{\pi}\tau_0 e \mathcal{E}_0}{4E_g}\right)^2 \sum_m |\mathcal{M}_{nm}(\boldsymbol{q}, \theta)|^2, \qquad (3)$$

where $E_g = 1.9$ eV is the measured direct band gap, the sum is over the two valence bands, $m \in \{v_1, v_2\}$, and $\mathcal{M}_{nm}$ is the velocity matrix element describing the interband transition and is given as $\mathcal{M}_{nm}(\boldsymbol{q}, \theta) =$

$\langle\psi_n(\boldsymbol{q})|\hat{\boldsymbol{\epsilon}}(\theta)\cdot\boldsymbol{\nabla}_{\boldsymbol{q}}\hat{\mathcal{H}}_{\mathrm{BL}}|\psi_m(\boldsymbol{q})\rangle$. Note that, since we only consider the fully excited state and neglect relaxation in the model, we drop the dependence on Δt. After summing over the possible transitions from the VB to the two-fold degenerate CB, we can formally write the excited state population as [34]

$$f^{exc}(\boldsymbol{q},\theta) \propto 1 + f_{\mathrm{lin}}(\boldsymbol{q})\cos(2\theta) + f_{\mathrm{circ}}(\boldsymbol{q})\sin(2\theta), \quad (4)$$

where f_{lin} and f_{circ} are spin-, valley- and momentum-dependent pre-factors that determine the weight between the linear ($\cos(2\theta)$) and circular ($\sin(2\theta)$) dichroism terms.

We calculate the intensity using Eq. (1) based on the assumption that the photoemitted electrons from the CB at $\boldsymbol{q}$ stem exclusively from pumping into this state and not from the decay of higher lying states. In our case, this is a justified assumption because of the resonant pumping condition. Moreover, we neglect many-body interactions and therefore disregard any recombination effects. Since our TR-ARPES spectra were collected along the $\bar{\Gamma}$-$\bar{\mathrm{K}}$ direction and the dichroism was extracted for a k-range covering the CBM, we calculate the intensity resulting from the resonant excitation to the CB at $q_y = 0$ and sum over q_x from -0.22 to 0.22 Å^{-1} for all possible pump pulse polarization angles, as shown for both SL and BL MoS_2 in Fig. 2(c). Our model recovers strong circular dichroism in SL MoS_2 (valley-polarization), but with a slightly asymmetric polarization-dependence due to a finite contribution from the linear dichroism term in Eq. (4) at finite $\boldsymbol{q}$. In BL MoS_2 the circular dichroism term is absent, due to inversion symmetry, and we only observe the $\cos(2\theta)$ dependence.

The complete (q_x, q_y)-dependent photoemission intensity in the CB of BL MoS_2 is shown for p- and s-polarized excitations in Figs. 2(d)-(e), respectively. The intensity difference between these cuts is shown in Fig. 2(f), where the blue (red) color signifies a negative (positive) sign corresponding to a momentum-dependent linear dichroism effect. Neglecting spin-orbit coupling and trigonal warping, the leading intralayer contribution to this momentum-resolved linear dichroism is

$$f_{\mathrm{lin}}(\boldsymbol{q}) \approx 2\frac{t_1^2 - 2E_0E_g}{E_g^2}q^2\cos(2\phi), \quad (5)$$

where t_1 is the intralayer effective hopping parameter which we set equal to 2.0 eV, $\phi = \arctan(q_y/q_x)$ is the azimuthal angle of vector $\boldsymbol{q}$ and $E_0 = 3\hbar^2/4\mu a^2$ with the reduced mass of electron-hole pairs given as $\mu \sim 0.15m_0$. The interlayer coupling term ($\hat{\mathcal{H}}_\perp$) in Eq. (2) cancels after summing over the optical transitions to the two-fold degenerate CB. Furthermore, Eq. (5) shows that linear dichroism only appears at finite momentum (q), that it cancels when azimuthally averaging over momentum and that the modulation depends on the intralayer interaction strength t_1. Finally, circular dichroism is absent in a perfectly inversion-symmetric BL when neglecting external influences, because $f_{\mathrm{circ}}(\boldsymbol{q}) \approx \tau_z(-\tau_z)$ for the bottom (top) layer, and thus $\tau_z + (-\tau_z) = 0$ when summing over layers.

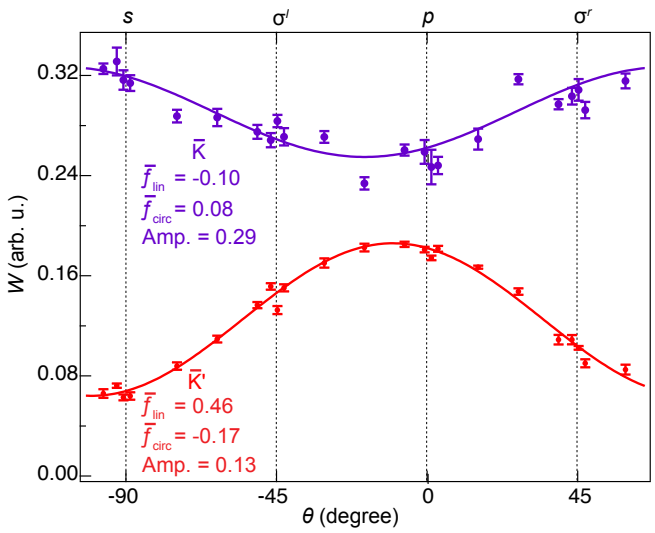

FIG. 3. Spectral weight W (markers) in the CB as a function of polarization angle θ measured at $\bar{\mathrm{K}}'$ (red) and $\bar{\mathrm{K}}$ (purple). Curves represent fits of the energy- and k-integrated photoemission intensity incorporating our model for the excited-state population in Eq. (4) with the given pre-factors and amplitude (Amp.).

The general form of the occupation function written in Eq. (4) shows that the intensity in polarization-dependent TR-ARPES spectra can be decomposed into linear and circular dichroism contributions. We explore this idea further by fitting the measured θ-dependent spectral weight (W) at the peak of the optical excitation to an energy- and k-integrated form of the intensity in Eq. (1) with the expression in Eq. (4) implemented. The spectral weight and the results of the fitting are presented at $\bar{\mathrm{K}}'$ and $\bar{\mathrm{K}}$ in Fig. 3. The fits provide the amplitudes $\bar{f}_{\mathrm{lin}}$ and $\bar{f}_{\mathrm{circ}}$, which represent an average over the k-range used to determine W. The values are stated in Fig. 3 and reveal that both the $\cos(2\theta)$- and $\sin(2\theta)$-terms are significant in our sample. The $\cos(2\theta)$-dependence is in agreement with the model around $\bar{\mathrm{K}}$ for BL MoS_2. The sign-change between $\bar{\mathrm{K}}'$ and $\bar{\mathrm{K}}$ of the $\cos(2\theta)$-terms is not explained by our simple model and may arise due to a strong anisotropy of the photoemission matrix element ($\mathcal{M}_n$) as described in Ref. 34. Many-body interactions such as carrier scattering between the two valleys and recombination can lead to additional contributions to the intensity that are neglected in our non-interacting model. The finite $\bar{f}_{\mathrm{circ}}$ could originate from symmetry breaking due to the substrate or due to the surface sensitivity of ARPES [42]. Note, however, that the latter effect would not be expected to lead to the observation of a *linear*

dichroism. Indeed, if the ARPES signal was completely dominated by the first layer, one would expect similar results for a single layer [19, 20], bilayer and bulk [17]. This is clearly not the case. Substrate-induced symmetry breaking, on the other hand, is expected to be rather minor because the substrate is known to have only a small effect on the electronic structure and spin texture of SL TMDCs on noble metal surfaces, since the region around $\bar{\mathrm{K}}$ falls into a projected band gap of the substrate [43, 44]. Finally, deviations from the ideal case could here also be caused by a minor presence of single-domain SL MoS_2 areas on the sample.

In summary, we observe momentum-resolved linear dichroism associated with optically excited electrons in the CB of BL MoS_2. Using a model to account for the polarization in both steps of our photoemission pump-probe experiment, we show that this can be linked to the intralayer single-electron hopping in the system. Exploiting the polarization of both pulses governing the optical excitation and subsequent photoemission in TR-ARPES offers an intriguing possibility to extract information about the electronic wave functions involved in the processes. The utility of this approach extends beyond valley dependent selection rules to studies of complex topological properties of unoccupied states such as the Berry curvature.

We thank Phil Rice and Alistair Cox for technical support during the Artemis beamtime. We gratefully acknowledge funding from VILLUM FONDEN through the Young Investigator Program (Grant. No. 15375) and the Centre of Excellence for Dirac Materials (Grant. No. 11744), the Danish Council for Independent Research, Natural Sciences under the Sapere Aude program (Grant No. DFF-4002-00029 and DFF-6108-00409) and the Aarhus University Research Foundation. Access to the Artemis Facility was funded by STFC. H.R. acknowledges the support from the Swedish Research Council (VR 2018-04252). I.M. acknowledges financial support by the International Max Planck Research School for Chemistry and Physics of Quantum Materials (IMPRS-CPQM).

* These authors contributed equally to the work.
† current address: Department of Physics, University of Trieste, Via Valerio 2,Trieste 34127, Italy
‡ Electronic address: ulstrup@phys.au.dk

[1] B. Henderson and G. F. Imbusch, *Optical Spectroscopy of Inorganic Solids* (Oxford University Press, 2006).
[2] W. Eberhardt and E. W. Plummer, Physical Review B **21**, 3245 (1980).
[3] I. Gierz, M. Lindroos, H. Höchst, C. R. Ast, and K. Kern, Nano Letters **12**, 3900 (2012).
[4] Z.-H. Zhu, C. N. Veenstra, G. Levy, A. Ubaldini, P. Syers, N. P. Butch, J. Paglione, M. W. Haverkort, I. S. Elfimov, and A. Damascelli, Phys. Rev. Lett. **110**, 216401 (2013).
[5] Y. Cao, J. A. Waugh, X.-W. Zhang, J.-W. Luo, Q. Wang, T. J. Reber, S. K. Mo, Z. Xu, A. Yang, J. Schneeloch, G. D. Gu, M. Brahlek, N. Bansal, S. Oh, A. Zunger, and D. S. Dessau, Nature Physics **9**, 499 EP (2013).
[6] M. Schüler, U. D. Giovannini, H. Hübener, A. Rubio, M. A. Sentef, and P. Werner, "Local berry curvature signatures in dichroic angle-resolved photoelectron spectroscopy," (2019), arXiv:1905.09404.
[7] S. Cho, J.-H. Park, J. Hong, J. Jung, B. S. Kim, G. Han, W. Kyung, Y. Kim, S.-K. Mo, J. D. Denlinger, J. H. Shim, J. H. Han, C. Kim, and S. R. Park, Phys. Rev. Lett. **121**, 186401 (2018).
[8] D. Xiao, G.-B. Liu, W. Feng, X. Xu, and W. Yao, Phys. Rev. Lett. **108**, 196802 (2012).
[9] K. F. Mak, K. L. McGill, J. Park, and P. L. McEuen, Science **344**, 1489 (2014).
[10] K. Mak, K. He, J. Shan, and T. Heinz, Nature Nanotechnology **7**, 494 (2012).
[11] H. Zeng, J. Dai, W. Yao, D. Xiao, and X. Cui, Nature Nanotech. **7**, 490 (2012).
[12] L. Perfetti, P. A. Loukakos, M. Lisowski, U. Bovensiepen, H. Eisaki, and M. Wolf, Physical Review Letters **99**, 197001 (2007).
[13] E. Malic, T. Winzer, E. Bobkin, and A. Knorr, Phys. Rev. B **84**, 205406 (2011).
[14] T. Rohwer, S. Hellmann, M. Wiesenmayer, C. Sohrt, A. Stange, B. Slomski, A. Carr, Y. Liu, L. M. Avila, M. Kallane, S. Mathias, L. Kipp, K. Rossnagel, and M. Bauer, Nature **471**, 490 (2011).
[15] J. C. Johannsen, S. Ulstrup, F. Cilento, A. Crepaldi, M. Zacchigna, C. Cacho, I. C. E. Turcu, E. Springate, F. Fromm, C. Raidel, T. Seyller, F. Parmigiani, M. Grioni, and P. Hofmann, Physical Review Letters **111**, 027403 (2013).
[16] A. Grubišić Čabo, J. A. Miwa, S. S. Grønborg, J. M. Riley, J. C. Johannsen, C. Cacho, O. Alexander, R. T. Chapman, E. Springate, M. Grioni, J. V. Lauritsen, P. D. C. King, P. Hofmann, and S. Ulstrup, Nano Lett. **15**, 5883 (2015).
[17] R. Bertoni, C. W. Nicholson, L. Waldecker, H. Hübener, C. Monney, U. D. Giovannini, M. Puppin, M. Hoesch, E. Springate, R. T. Chapman, C. Cacho, M. Wolf, A. Rubio, and R. Ernstorfer, Phys. Rev. Lett. **117**, 277201 (2016).
[18] S. Aeschlimann, R. Krause, M. Chávez-Cervantes, H. Bromberger, R. Jago, E. Malić, A. Al-Temimy, C. Coletti, A. Cavalleri, and I. Gierz, Phys. Rev. B **96**, 020301 (2017).
[19] S. Ulstrup, A. Grubišić Čabo, D. Biswas, J. M. Riley, M. Dendzik, C. E. Sanders, M. Bianchi, C. Cacho, D. Matselyukh, R. T. Chapman, E. Springate, P. D. C. King, J. A. Miwa, and P. Hofmann, Phys. Rev. B **95**, 041405 (2017).
[20] H. Beyer, G. Rohde, A. Grubišić Čabo, A. Stange, T. Jacobsen, L. Bignardi, D. Lizzit, P. Lacovig, C. E. Sanders, S. Lizzit, K. Rossnagel, P. Hofmann, and M. Bauer, in press, Phys. Rev. Lett. (2019), 1907.10553.
[21] M. Dendzik, A. Bruix, M. Michiardi, A. S. Ngankeu, M. Bianchi, J. A. Miwa, B. Hammer, P. Hofmann, and C. E. Sanders, Phys. Rev. B **96**, 235440 (2017).
[22] A. Baraldi, G. Comelli, S. Lizzit, M. Kiskinova, and G. Paolucci, Surface Science Reports **49**, 169 (2003).

[23] "See Supplemental Material for details of sample growth and X-ray photoelectron diffraction data on the distribution of BL MoS_2 domain orientations, for high resolution ARPES measurements, for TR-ARPES experimental details and for full details on the Hamiltonian and tight binding parameters applied in the model.".

[24] M. Baker, R. Gilmore, C. Lenardi, and W. Gissler, Applied Surface Science **150**, 255 (1999).

[25] F. J. García de Abajo, M. A. Van Hove, and C. S. Fadley, Phys. Rev. B **63**, 075404 (2001).

[26] S. S. Grønborg, S. Ulstrup, M. Bianchi, M. Dendzik, C. E. Sanders, J. V. Lauritsen, P. Hofmann, and J. A. Miwa, Langmuir **31**, 9700 (2015).

[27] M. Dendzik, M. Michiardi, C. Sanders, M. Bianchi, J. A. Miwa, S. S. Grønborg, J. V. Lauritsen, A. Bruix, B. Hammer, and P. Hofmann, Phys. Rev. B **92**, 245442 (2015).

[28] H. Bana, E. Travaglia, L. Bignardi, P. Lacovig, C. E. Sanders, M. Dendzik, M. Michiardi, M. Bianchi, D. Lizzit, F. Presel, D. D. Angelis, N. Apostol, P. K. Das, J. Fujii, I. Vobornik, R. Larciprete, A. Baraldi, P. Hofmann, and S. Lizzit, 2D Materials **5**, 035012 (2018).

[29] D. Woodruff, Surf. Sci. Rep. **62**, 1 (2007).

[30] J. B. Pendry, Journal of Physics C: Solid State Physics **13**, 937 (1980).

[31] J. He, K. Hummer, and C. Franchini, Phys. Rev. B **89**, 075409 (2014).

[32] S. V. Hoffmann, C. Søndergaard, C. Schultz, Z. Li, and P. Hofmann, Nucl. Instr. and Meth. Phys. Res. A **523**, 441 (2004).

[33] S. Ulstrup, J. C. Johannsen, A. Crepaldi, F. Cilento, M. Zacchigna, C. Cacho, R. T. Chapman, E. Springate, F. Fromm, C. Raidel, T. Seyller, F. Parmigiani, M. Grioni, and P. Hofmann, Journal of Physics: Condensed Matter **27**, 164206 (2015).

[34] H. Rostami, K. Volckaert, N. Lanata, S. K. Mahatha, C. E. Sanders, M. Bianchi, D. Lizzit, L. Bignardi, S. Lizzit, J. A. Miwa, A. V. Balatsky, P. Hofmann, and S. Ulstrup, "Layer and orbital interference effects in photoemission from transition metal dichalcogenides," (2019), arXiv:1910.01882 [cond-mat.mtrl-sci].

[35] S. Moser, Journal of Electron Spectroscopy and Related Phenomena **214**, 29 (2017).

[36] A. Kormányos, V. Zólyomi, N. D. Drummond, P. Rakyta, G. Burkard, and V. I. Fal'ko, Phys. Rev. B **88**, 045416 (2013).

[37] H. Rostami, A. G. Moghaddam, and R. Asgari, Phys. Rev. B **88**, 085440 (2013).

[38] H. Rostami, R. Asgari, and F. Guinea, Journal of Physics: Condensed Matter **28**, 495001 (2016).

[39] Z. Gong, G.-B. Liu, H. Yu, D. Xiao, X. Cui, X. Xu, and W. Yao, Nature Communications **4**, 2053 (2013).

[40] A. Kormányos, V. Zólyomi, V. I. Fal'ko, and G. Burkard, Phys. Rev. B **98**, 035408 (2018).

[41] H. Haug and S. Koch, *Quantum Theory of the Optical and Electronic Properties of Semiconductors: Fourth Edition* (World Scientific Publishing Company, 2004).

[42] J. M. Riley, F. Mazzola, M. Dendzik, M. Michiardi, T. Takayama, L. Bawden, C. Granerod, M. Leandersson, T. Balasubramanian, M. Hoesch, T. K. Kim, H. Takagi, W. Meevasana, P. Hofmann, M. S. Bahramy, J. W. Wells, and P. D. C. King, Nature Physics **10**, 835 (2014).

[43] J. A. Miwa, S. Ulstrup, S. G. Sørensen, M. Dendzik, A. G. Čabo, M. Bianchi, J. V. Lauritsen, and P. Hofmann, Phys. Rev. Lett. **114**, 046802 (2015).

[44] P. Eickholt, C. Sanders, M. Dendzik, L. Bignardi, D. Lizzit, S. Lizzit, A. Bruix, P. Hofmann, and M. Donath, Phys. Rev. Lett. **121**, 136402 (2018).